Radiocarbon, Vol 60, Nr 3, 2018, p 775–790 DOI:10.1017/RDC.2018.22

DIMENSIONS OF RADIOCARBON VARIABILITY WITHIN SEDIMENTARY ORGANIC MATTER

Rui Bao[1,2,3*] • Ann P McNichol[2] • Cameron P McIntyre[1,4,5] • Li Xu[2] • Timothy I Eglinton[1]

[1]Geological Institute, ETH Zurich, Zurich, Switzerland.
[2]National Ocean Sciences Accelerator Mass Spectrometry Facility, Woods Hole Oceanographic Institution, Woods Hole, Massachusetts, USA.
[3]Present address: Department of Earth and Planetary Sciences, Harvard University, Cambridge, Massachusetts, USA.
[4]Laboratory for Ion Beam Physics, ETH Zurich, Zurich, Switzerland.
[5]Scottish Universities Environmental Research Centre, Glasgow, United Kindom.

ABSTRACT. Organic carbon (OC) radiocarbon (^{14}C) signatures in marine surface sediments are highly variable and the causes of this heterogeneity remain ambiguous. Here, we present results from a detailed ^{14}C-based investigation of an Arabian Sea sediment, including measurements on organic matter (OM) in bulk sediment, specific grain size fractions, and OC decomposition products from ramped-pyrolysis-oxidation (RPO). Our results show that ^{14}C ages of OM increase with increasing grain size, suggesting that grain size is an important factor controlling the ^{14}C heterogeneity in marine sediments. Analysis of RPO decomposition products from different grain size fractions reveals an overall increase in age of corresponding thermal fractions from finer to coarser fractions. We suggest that hydrodynamic properties of sediment grains exert the important control on the ^{14}C age distribution of OM among grain size fractions. We propose a conceptual model to account for this dimensionality in ^{14}C variability that invokes two predominant modes of OM preservation within different grain size fractions of Arabian Sea sediment: finer (<63 μm) fractions are influenced by OM-mineral grain aggregation processes, giving rise to relatively uniform ^{14}C ages, whereas OM preserved in coarser (>63 μm) fractions includes materials encapsulated within microfossils and/or entrained fossil (^{14}C-depleted) OC hosted in detrital mineral grains. Our findings highlight the value of RPO for assessment of ^{14}C age variability in sedimentary OC, and for assessing mechanisms of OM preservation in aquatic sediments.

KEYWORDS: Arabian Sea, grain size, hydrodynamic processes, organic matter, radiocarbon, ramped pyrolysis-oxidation.

INTRODUCTION

The radiocarbon (^{14}C) age of sedimentary organic matter (OM) is an important characteristic that can be exploited in studies of the contemporary and past oceanic carbon cycle. Several prior investigations have explored controls on the ^{14}C age distribution in marine sediments (e.g., Wakeham et al. 2009; Griffith et al. 2010; Bao et al. 2016). Such investigations have indicated that interactions between OM and minerals, which have been frequently inferred to exert a strong influence on OM preservation (Mayer 1994; Hedge and Keil 1995; Bergamaschi et al. 1997; Blair and Aller 2012), may further influence corresponding ^{14}C age characteristics of sedimentary OM (Hwang et al. 2010; Bao et al. 2016; Wakeham and Canuel 2016). While ^{14}C measurements on bulk OM can be used to understand the net ^{14}C age of all organic components, prior studies have demonstrated that further information can be gleaned from isotopic analysis of specific organic components separated from bulk OM (Trumbore and Zheng 1996; Eglinton et al. 1997; Wakeham et al. 2009).

Ocean sediments are composed of a spectrum of grain sizes that reflects source inputs, depositional and sedimentological conditions. Consequently, ^{14}C contents of OM in different grain size fractions may be one of the factors influencing bulk ^{14}C ages. Cathalot et al. (2013) showed that ^{14}C ages of OM are related to the percentage of finer fractions (<63 μm) in bulk coastal sediments. However, while prior studies have examined ^{14}C variations in organic carbon (OC) associated with specific size or density fractions of soil or marine sediments (Trumbore and Zheng 1996; Megens et al. 2002; Wakeham et al. 2009; Bao et al. 2016), an assessment of underlying ^{14}C age variability within specific grain size fractions has not been undertaken yet may shed new light on OM sources and mechanisms of preservation.

*Corresponding author. Email: rui_bao@fas.harvard.edu.

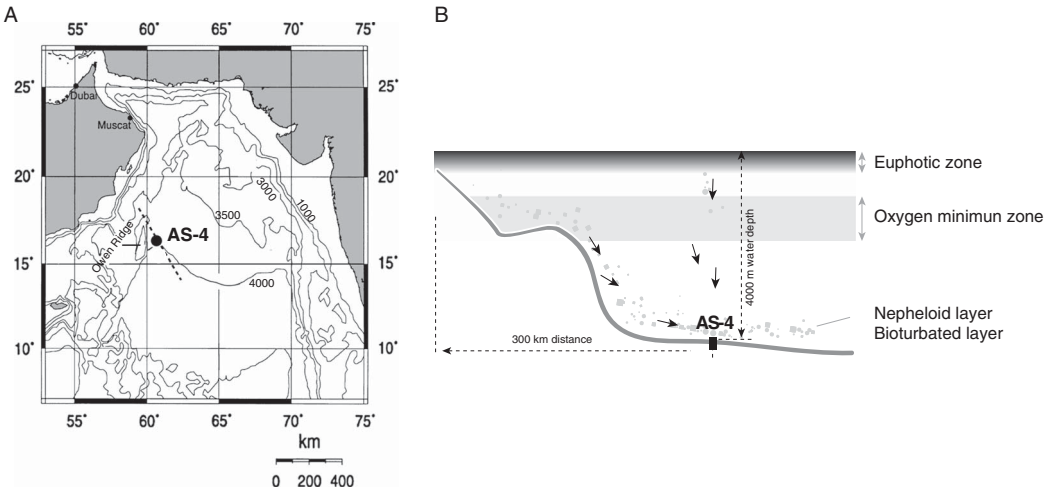

Figure 1 (A) Sample location in the NW Arabian Sea (modified from Schnetger et al. 2000); (B) schematic water column cross-section showing characteristic features, including the oxygen minimum (deficient) zone, and nepheloid layers, the arrows show the sediment transport (modified after Pfannkuche and Lochte 2000).

Recently, ramped pyrolysis-oxidation (RPO) analysis was developed at the National Ocean Sciences Accelerator Mass Spectrometry (NOSAMS) facility, Woods Hole Oceanographic Institution (WHOI) (Rosenheim et al. 2008; Hemingway et al. 2017; Zigah et al. 2017; Bao et al. 2018). This technique allows separation of OM components in a sample based on thermochemical stability in response to exposure to a linear temperature gradient (Rosenheim and Galy 2012). Simultaneous oxidation of thermal decomposition products yields CO_2 that can be trapped and subsequently analyzed for its carbon isotopic (including ^{14}C) composition. Application of the RPO technique to marine sedimentary OM has revealed marked heterogeneity in ^{14}C ages among different thermal windows within the RPO thermograms (Schreiner et al. 2014), shedding new light on ^{14}C age distribution within OC. Here, we examine ^{14}C ages of OM associated with different grain size fractions in a surficial sediment sample from the northwestern Arabian Sea (Figure 1). We further explore the spectrum of ^{14}C ages exhibited by different organic components residing in each grain size fraction using RPO in order to develop improved insights about the processes contributing to OC ^{14}C ages observed at the bulk level.

MATERIAL AND METHODS

Background and Sampling

The northwestern Arabian Sea is characterized by high nutrient concentrations in surface waters that drives high biological productivity and is accompanied by a well-developed subsurface oxygen minimum zone (OMZ) (Morrison et al. 1998, 1999; Pfannkuche and Lochte 2000) (Figure 1b). This combination of properties results in high OC burial in underlying sediments (~3.2 g C m^{-2} yr^{-1}; Pfannkuche and Lochte 2000; Boetius et al. 2000a, 2000b; Schnetger et al. 2000). Upwelling conditions also give rise to large fluxes of biogenic opal to the sediments (~14.1 g m^{-2} yr^{-1}, Haake et al. 1993) as a result of the prominence of diatoms in the phytoplankton community and opal concentrations in sediments are further enriched by preferential decomposition of OC compared to opal dissolution (Grandel et al. 2000). Turbidites are observed in underlying sediments located in the eastern Owen Ridge, characterized by carbonate-rich and pelagic sediments but with enriched in OC contents (Schnetger et al. 2000).

https://doi.org/10.1017/RDC.2018.22 Published online by Cambridge University Press

According to results of Schnetger et al. (2000), a sedimentation rate on the top of Owen Ridge is ~3 cm/ky. A markedly higher sedimentation rate can thus be expected in the eastern flank of Owen Ridge (Kraal et al. 2012). The underlying sediments in this area are characterized by low bioturbation rates, shallow depth of mixing layer (~5 cm; Turnewitsch et al. 2000), and shallow oxygen penetration depths (~2 cm; Grandel et al. 2000). These characteristics suggest minimal biological or physical disturbance of sediments in this area (Turnewitsch et al. 2000; Pfannkuche and Lochte 2000).

We obtained a sediment core (AS-4, 15.9945ºN, 61.5333ºE, 3985 m water depth) from the eastern flank of Owen Ridge using a box corer during R/V Thomas Thompson cruise TTN041, in November 1994 (Figure 1). One sediment section (2–10 cm) that was frozen until this analysis was selected for investigation as sufficient material was available for in-depth analysis. Upon thawing, the sample (~10 g) was wet sieved into 6 grain size fraction: <32 μm, 32–63 μm, 63–125 μm, 125–250 μm, 250–500 μm, and >500 μm fractions using ~200 mL Milli-Q water through stainless steel mesh sieves in less than 1 hr (in order to minimize OM losses). An aliquot of the <32 μm fraction was further sieved into <20 μm and 20–32 μm, and the latter fractions were subsequently only processed for ^{14}C analysis. Bulk sediment samples and grain size fractions were then freeze-dried prior to analysis.

Mineral Surface Area, Grain Size Distribution, Scanning Electron Microscopy

Aliquots (~1 g dw) of freeze-dried samples were heated at 350°C for 24 hr to remove OM (Mayer 1994). The samples were subsequently outgassed at 350°C under vacuum for 2 hr to ensure complete removal of moisture, and mineral-specific surface area (SA) measured using a 5-point Brunauer–Emmett–Teller (BET) method on a NOVA 4000 surface area analyzer (Quantachrome Instruments) (Keil et al. 1994, 1997; Mayer 1994; Tao et al. 2016). Grain size analysis was performed on bulk sediment for mass percentage using a Mastersizer 2000 (Malvern Instruments Ltd) laser-diffraction instrument at Geological Institute, ETH-Zurich (Tao et al. 2016). The individual sample image (scanning electron microscope; SEM) was performed at Scientific Center for Optical and Electron Microscopy (FEI Quanta 200F) of ETH Zurich (SEM images are shown in Supplementary Figure 1).

Acidification

Different laboratories utilize different acidification methods to remove carbonate from sediment samples prior to elemental and carbon isotope analysis. At ETH Zurich, HCl fumigation was chosen to remove inorganic carbon (Bao et al. 2016), whereas HCl rinsing was the applied pretreatment at NOSAMS (McNichol et al. 1994).

Method 1, Fumigation (ETH Zurich)

Freeze-dried samples were weighed into Ag capsules. A beaker filled with 37 % HCl was placed at the bottom of a glass desiccator; the samples were placed on a ceramic tray above the acid. The desiccator was evacuated and the samples were heated at 60°C for 72 hr. The HCl was subsequently replaced with a beaker containing NaOH pellets, and the desiccator was again evacuated and placed at 60°C, for 72 hr in order to neutralize any excess acid. This "fumigation" pretreatment process was conducted at ETH Zurich.

Method 2, HCl Rinsing (NOSAMS)

Bulk and grain size fraction samples were treated with 1N HCl and then rinsed with Milli-Q water to remove the inorganic carbon at NOSAMS prior to further analysis. All glassware used

https://doi.org/10.1017/RDC.2018.22 Published online by Cambridge University Press

during this "HCl rinsing" process was precombusted at 550°C for 5 hr prior to use. Each sample (>100 mg dry weight) was weighed into a 60 mL glass centrifuge tube and 10 mL of 1.0 N HCl was added (Fisher Trace Metal Grade, A508-P212). After gentle agitation, the glass tubes were placed in a 60°C water bath (1 hr). The samples were then centrifuged (2500 rpm) to separate the supernatants and solid materials. To remove residual acid, Milli-Q water (10 mL) was added to the centrifuge tubes, which were then agitated, centrifuged, and decanted as above (repeated three times). Finally, the solid samples (residues) were vacuum-filtered onto a precombusted GF/F filter (0.7 μm) using a glass funnel, placed in glass petri dish, and dried (60°C, 24 hr).

Bulk and Grain Size-Specific Organic Geochemistry

Fumigated samples were analyzed for organic carbon content (TOC), and carbon isotope composition at ETH Zurich. These samples (except <20 μm and 20–32 μm fractions) were prepared for ^{14}C analysis using an automated graphitization system at the Laboratory of Ion Bean Physics, ETH Zurich (AGE 3, Ionplus AG, Switzerland). Corresponding ^{13}C compositions and TOC contents were measured at the Stable Isotope Laboratory of Geological Institute, ETH Zurich. Corresponding $\delta^{13}C$ values were determined to a precision of better than ± 0.1‰. The HCl-rinsing samples and the fumigated <20 μm and 20–32 μm fractions were prepared via sealed tube combustion, and subsequently analyzed as CO_2 for ^{14}C using a mini radiocarbon dating system (MICADAS) at ETH Zurich (Ruff et al. 2007). All ^{14}C data are reported as fraction modern (Fm) and ^{14}C age (yr BP), as defined by Stuiver and Polach (1977).

Ramped Pyrolysis-Oxidation (RPO)

HCl-rinsing samples were weighed, loaded into a quartz reactor, and heated using a linear temperature program (5°C min^{-1}) from 150°C until a maximum of 895°C. Evolved volatile products (thermal decomposition fractions [T_n]) were simultaneously oxidized and removed from the reactor using a carrier gas mixture of O_2 and He (~8% O_2, 35 mL min^{-1} total flow rate). A continuous record of evolved CO_2 was obtained via a flow-through infrared CO_2 analyzer (Sable Systems International Inc., CA-10a), before CO_2 derived from thermally volatilized components was sequentially collected in 5–7 temperature windows (intervals) (T_n: 150–300°C, 300–371°C, 371–414°C; 414–462°C, 462–507°C, 507–556°C, 556–896°C). For the 20–32 μm and 63–125 μm grain size fractions, evolved products from two thermal windows (462–507°C, 507–556°C) were tapped into a single fraction (i.e., 462–556°C), due to limited amounts of CO_2. For the 32–63 μm grain size fraction, evolved products from three thermal windows (462–507°C, 507–556°C, 556–896°C) were trapped into a single fraction (462–896°C). After isolation of evolved products corresponding to these thermal windows, the CO_2 was further distilled and quantified manometrically using standard vacuum line techniques (McNichol et al. 1994). Resulting CO_2 samples were then trapped into precombusted glass tubes with ~50 mg CuO and ~10 mg Ag granules and combusted (525°C, 5 hr) as a final gas purification step prior to isotopic measurement. RPO analysis was performed at NOSAMS and ^{14}C measurements of evolved CO_2 were analyzed using the ETH Zurich MICADAS.

RESULTS

Analysis of Grain Size Fractions

The majority of sediment mass occurs in the 63–125 μm grain size fraction (Table 1 and Figure 2), accounting for >40% of the bulk sample. The <32 μm and 32–63 μm are the next most abundant, collectively accounting for ~35% of the mass. The mass percentage decreases with increasing grain size in the >63 μm size range. With respect to mineral-specific SA (Table 1 and Figure 2), the bulk SA is 16.2 m^2/g, with the 32–63 μm fraction exhibiting the lowest value

https://doi.org/10.1017/RDC.2018.22 Published online by Cambridge University Press

Table 1 Organic geochemical data for fumigated grain size fractions.

	Mass %	OC (wt %)	SA (m^2/g)	OC/SA (mg C/m^2)	$\delta^{13}C$ (‰)	^{14}C age (yr BP) # (fumigated samples)	^{14}C age (yr BP) (HCl-rinsing samples)
<32 μm	17	5.5	22	2.5	–21.4	763 ± 51	942 ± 91§
32–63 μm	21	0.4	7.5	0.5	–22.5	1157 ± 56	1382 ± 97
63–125 μm	46	0.3	10.0	0.3	–22.0	1620 ± 53	1946 ± 88
125–250 μm	11	2.3	32.0	0.7	–20.7	2306 ± 53	2472 ± 96
250–500 μm	5	1.1	31.2	0.4	–20.8	2686 ± 54	3178 ± 91
>500 μm	<1	2.2	—	—	–19.1	3958 ± 92	—
Bulk		2.1	16.2	1.3	–21.2	1455 ± 53	1537 ± 96

§Indicates that ^{14}C age of <32 μm fraction was calculated by measured ^{14}C ages of <20 μm (892 ± 91 yr BP) and 20–32 μm fractions (1071 ± 91 yr BP), and their mass %.
#For fumigation samples, <20 μm and 20–32 μm fractions were also measured for ^{14}C ages, 675 ± 76 yr BP, 747 ± 81 yr BP, respectively.

(7.5 m^2/g) and the 125–250 μm fraction yielding the highest value (32.0 m^2/g). The 250–500 μm fraction also has a relatively high SA, whereas SA values for the <32 μm and 63–125 μm fractions are 22 m^2/g and 10.0 m^2/g, respectively.

Fumigation Samples

The maximum %OC (5.5%) is found in the finest fraction (<32 μm), while %OC values of other fractions range between 0.3 % to ~ 2.3 %, with the 32–63 μm and 63–125 μm fractions exhibiting the lowest %OC values (Table 1 and Figure 2). The bulk OC content of the sample is 21 mg/gdw with the largest proportion of the TOC residing in the <32 μm fraction (~64%), with lesser amounts in the 63–125 μm and 125–250 μm fractions (~9% and ~17%, respectively; Figure 2). Correspondingly, the <32 μm fraction exhibits the maximum OC:SA ratio (2.5 mg C/m^2), while other fractions are markedly lower (≤0.7 mg C/m^2).

Acid-fumigated samples were analyzed for ^{13}C and ^{14}C composition of OC. The $\delta^{13}C$ value of the bulk OC is –21.2‰, similar to that of the <32 μm fraction (–21.5‰, Figure 2). The 32–63 μm and 63–125 μm fractions exhibit lower $\delta^{13}C$ values, –22.5‰ and –22.0‰, respectively, whereas the coarser fractions (125–250 μm, 250–500 μm, and >500 μm) exhibit higher $\delta^{13}C$ values (–20.7‰, –20.8‰, and –19.1‰, respectively). Corresponding ^{14}C results (bulk ^{14}C age, 1455 ± 53 yr BP) reveal a clear trend of increasing ^{14}C ages (decreasing Fm) with increasing grain size (Figure 3), the <32 μm fraction being the youngest (763 ± 53 yr BP) and the >500 μm fraction being the oldest (3958 ± 92 yr BP). The integrated ^{14}C age taking into account mass balance and OC contents of grain size fractions is 1506 ± 53 yr BP, similar to the measured bulk age (1455 ± 53 yr BP). The former agrees with the latter within error, suggesting that any redistribution of OM across the grain size fractions during sample preparation does not significantly affect the ^{14}C results.

HCl-Rinsing Samples

Samples subjected to carbonate removal via HCl rinsing exhibit ^{14}C ages similar to those subjected to acid fumigation (Figure 3). The youngest ^{14}C age (892 ± 91 yr BP) is found in finest (<20 μm fraction), while the 250–500 μm fraction exhibits the oldest ^{14}C age (3178 ± 91 yr BP; >500 μm fraction was not measured). Notably, however, all the individual grain size fractions

https://doi.org/10.1017/RDC.2018.22 Published online by Cambridge University Press

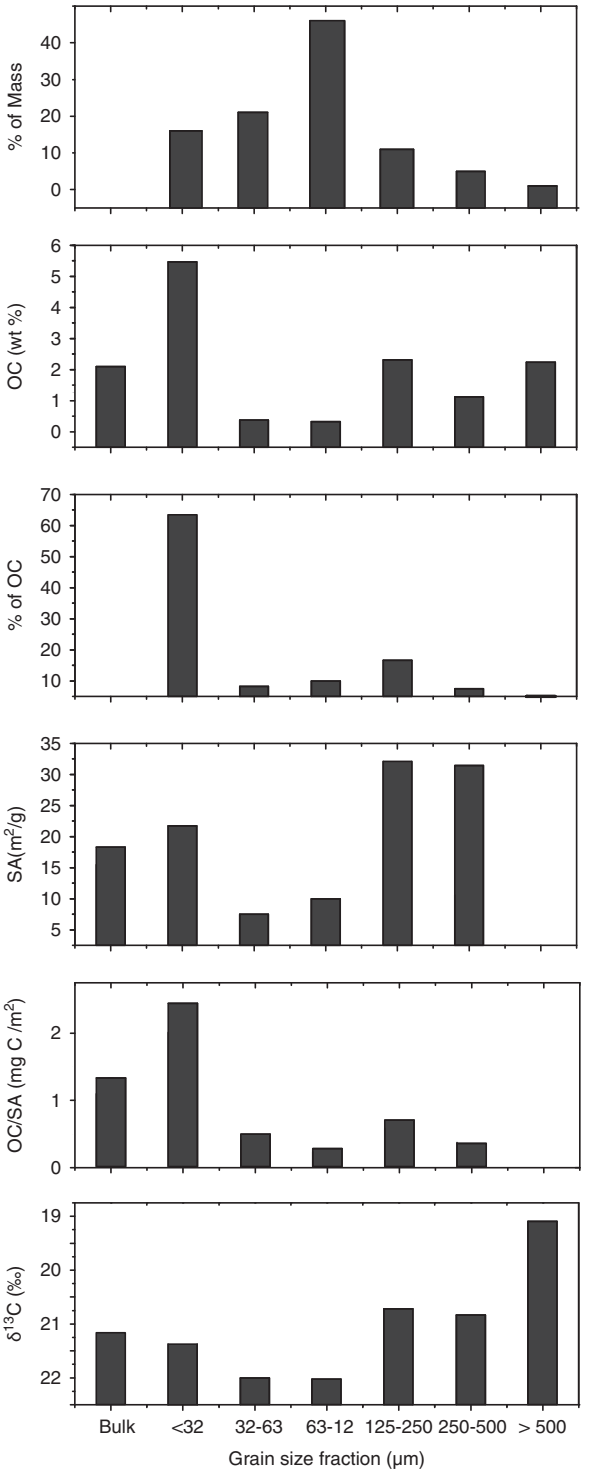

Figure 2 Histograms of sediment mass percentage (% of mass), mineral-specific surface area (SA), and organic geochemical characteristics of individual grain size fractions (fumigated samples) in the Arabian Sea sediment sample.

https://doi.org/10.1017/RDC.2018.22 Published online by Cambridge University Press

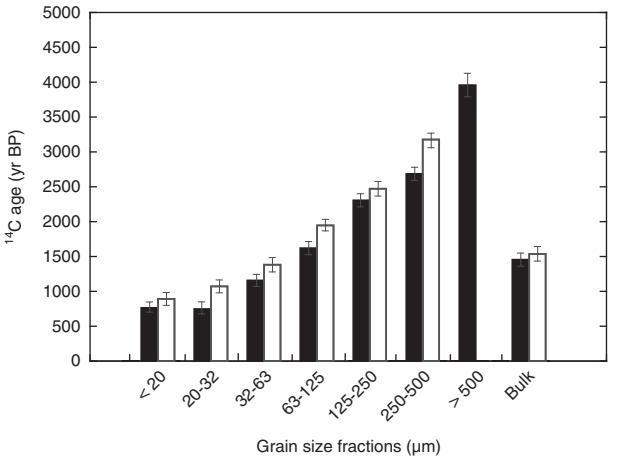

Figure 3 ^{14}C age characteristics of sedimentary OM as a function of grain size for fractions pretreated using the two acidification methods (black: fumigation; white: HCl rinsing). The >500 μm fraction was not acidified using HCl rinsing.

subjected to HCl rinsing exhibit systematically older ^{14}C ages than corresponding fumigation samples. The offsets range from 117 ± 167 yr (<20 μm fraction) to 582 ± 145 yr (250–500 μm fraction (Figure 3). While some of these observed differences between the fumigated and HCl-rinsing samples may reflect contrasting analytical and/or instrumental methods, this discrepancy is most likely due to preferential solubilization of labile (young) OC during the HCl-rinsing treatment (Komada et al. 2008; Brodie et al. 2011).

RPO Results

HCl-Rinsing Samples

RPO analyses of the individual grain size fractions processed using the HCl-rinsing method show the presence of two distinct peaks in the thermogram of each sample with consistent temperatures of maximum CO_2 generation (T_{max}, peak 1 and peak 2, ~320°C and ~440°C, respectively among samples (Figure 4), however relative peak heights differ markedly between grain size fractions. The overall similarity of the thermograms suggests similarities in thermochemical stability of OM. The finest fractions (<20 μm and 20–32 μm) exhibit near identical thermogram patterns, whereas the second thermal peak increases its relative height compared with that of the first thermal peak with increasing grain size from 63–125 μm to 250–500 μm (Figure 4).

Table 2 and Figure 5 show the variability in ^{14}C ages among thermal windows obtained from different grain size fractions. These range from 700 ± 76 yr BP to 3721 ± 91 yr BP. Analysis of thermally resolved OM decomposition products from different grain size fractions reveals an overall increase in age of corresponding thermal decomposition products from finer to coarser fractions (Figure 5). Generally, thermal windows from the relatively fine grain size fractions (<63 μm fractions and/or 63–125 μm fraction) exhibit relatively uniform ^{14}C ages, especially for the lower thermal windows (i.e., those evolving at <500°C; Figure 5). In contrast, thermal windows exhibit a general increase in ^{14}C ages with increasing temperature for coarser grain size fractions (>125 μm). One exception to the general trend of increasing age with increasing temperature of thermal windows from coarser particles is thermal window 6 (507–556°C, blue bar), and thermal window 5' (462–556°C, pink bar) (Figure 5). Similarly, Rosenheim et al. (2008) found that Antarctic sediments also exhibited lower ^{14}C age in the ~520–560°C thermal

https://doi.org/10.1017/RDC.2018.22 Published online by Cambridge University Press

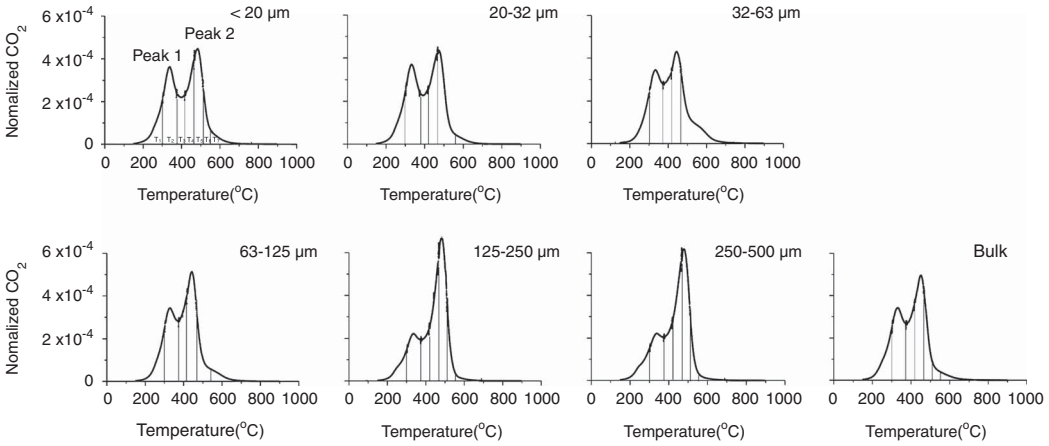

Figure 4 Thermograms of OM from different grain size fractions and bulk sample (pretreated by HCl rinsing). Vertical lines show the temperature windows. Taking <20 μm fraction as an example, peak 1 and peak 2, and thermal windows ($T_{1\text{-}7}$) are labeled.

window relative to its neighbor thermal windows. This suggests that some thermally refractory OM associated with all grain size fractions may exhibit relatively young ^{14}C ages. Nevertheless, overall ^{14}C ages of corresponding thermal windows from each sample exhibit a step-wise increase from finer (<20 μm and 20–32 μm) to coarser fractions, consistent with bulk ^{14}C ages of the grain size fractions.

DISCUSSION

The OM in the different grain size fractions of sediment sample AS-4 exhibits a range of properties (Figure 2). Generally, relatively high $\delta^{13}C$ values (–22.5‰ to –19.1‰) suggest that marine OC represents the dominant OC source in all fractions (Table 1), however the range in ^{14}C ages (763 ± 51 to 3958 ± 53 ^{14}C yr BP), suggests that this OM has experienced diverse pre and post-depositional processing and fates. We note that the 32–63 μm and 63–125 μm fractions have lower $\delta^{13}C$ values, as well as lower SA values, compared to both corresponding finer and coarser fractions (Figure 2). SA has previously been argued to play an important role in preservation of sedimentary OM (e.g., Mayer 1994). In this study, we find that SA displays a positive relationship with $\delta^{13}C$ values (SA vs. $\delta^{13}C$, $r^2 = 0.97$, not-shown), implying that SA may be linked to either OC source or the preferential degradation/preservation of specific molecules in the corresponding materials (Wang et al. 1996, 1998; Wang and Druffel 2001; Hwang and Druffel 2003).

SEM images of grain size fractions reveal the presence of small aggregates of OM and other biological detritus (e.g., diatom frustules, coccoliths) in the <32 μm fraction, Supplementary Figure 1S). Similar aggregates were also observed in the low-density fraction (fine fraction) of sediments from the oxygen-deficient zone of the Eastern Pacific Ocean continental margin (Arnarson and Keil 2007). For these finer grain size fractions, we speculate that OM may be preserved both through close association with fine-grained, high SA particles (Mayer 1994; Wakeham et al. 2009), as well as via stabilization in aggregates (Arnarson and Keil 2007; Blair and Aller 2012). In contrast, the coarser fractions (e.g., 125–250 μm and 250–500 μm) contain abundant calcareous microfossils (e.g., foraminiferal tests, Supplementary Figure 1S). In contrast to detrital sand grains residing in such coarser grain-size fractions, these microfossils may contain abundant pore space within their biomineral matrix, with the latter serving both to

https://doi.org/10.1017/RDC.2018.22 Published online by Cambridge University Press

Table 2 Radiocarbon ages of thermal decomposition components in different grain size fractions of AS-4 sample.

Sample name	Faction	$F^{14}C$	Error	^{14}C (yr BP)	Error
<20 μm	frac1	0.8934	0.0085	905	77
	frac2	0.9034	0.0120	816	106
	frac3	0.9166	0.0086	700	76
	frac4	0.9051	0.0094	801	83
	frac5	0.9088	0.0091	768	81
	frac6	0.9437	0.0100	466	85
	frac7	0.8896	0.0101	940	91
20–32 μm	frac1	0.8948	0.0090	893	81
	frac2	0.9014	0.0097	834	87
	frac3	0.9058	0.0108	795	96
	frac4	0.8948	0.0100	893	90
	frac5'	0.9132	0.0096	730	84
	frac7	0.8535	0.0087	1272	82
32–63 μm	frac1	0.8347	0.0089	1451	86
	frac2	0.8673	0.0107	1144	100
	frac3	0.8470	0.0083	1334	79
	frac4	0.8557	0.0087	1252	82
	frac5"	0.8411	0.0081	1390	77
63–125 μm	frac1	0.7929	0.0080	1864	81
	frac2	0.7948	0.0085	1845	86
	frac3	0.7695	0.0094	2105	98
	frac4	0.7846	0.0084	1948	86
	frac5'	0.8197	0.0097	1597	95
	frac7	0.7276	0.0080	2555	88
125–250 μm	frac1	0.7783	0.0079	2014	82
	frac2	0.7556	0.0085	2252	90
	frac3	0.7459	0.0083	2355	90
	frac4	0.7199	0.0092	2640	102
	frac5	0.7156	0.0078	2688	87
	frac6	0.7698	0.0088	2102	92
	frac7	0.7370	0.0088	2451	96
250–500 μm	frac1	0.7241	0.0080	2594	88
	frac2	0.7199	0.0077	2640	86
	frac3	0.6712	0.0143	3203	171
	frac4	0.6628	0.0082	3304	99
	frac5	0.6652	0.0079	3274	95
	frac6	0.7316	0.0081	2511	89
	frac7	0.6284	0.0071	3731	91
Bulk	frac 1	0.8425	0.0084	1377	80
	frac 2	0.8282	0.0087	1515	84
	frac 3	0.8244	0.0081	1552	79
	frac 4	0.8127	0.0078	1666	77
	frac 5	0.8685	0.0082	1132	75
	frac 6	0.8686	0.0085	1131	78
	frac 7	0.8090	0.0078	1702	78

https://doi.org/10.1017/RDC.2018.22 Published online by Cambridge University Press

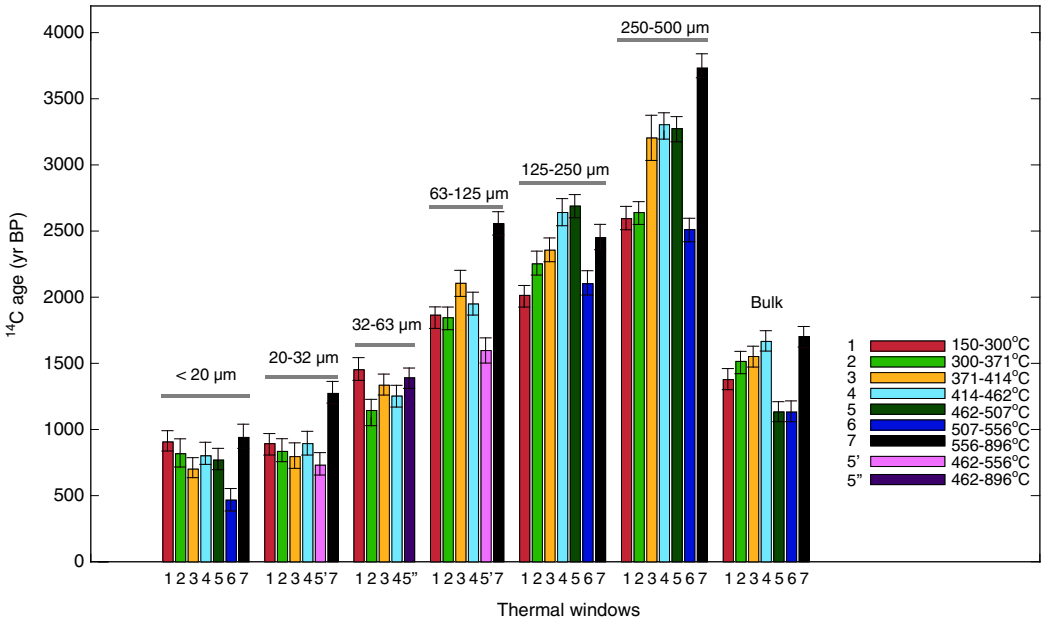

Figure 5 ^{14}C age spectrum among thermal windows from corresponding grain size fractions as well as the original bulk sample. The *x*-axis shows the number of thermal windows, and corresponding temperature intervals are indicated in Figure 4.

increase SA, and to protect OM intrinsic to (Ingalls et al. 2003) or associated with the biomineral host from degradation (Mayer 1994; Arnarson and Keil 2007; Wakeham et al. 2009). These different modes of SA-related protection in fine and coarse fractions may influence the content as well as ^{14}C age of the OM associated with specific grain size fractions.

Despite both fractions having relatively high SA (Figure 2), the ^{14}C ages of OC within the coarsest size fraction (250–500 µm, 2686 ± 54 yr BP) are substantially older than those in the finest fraction (<32 µm, 763 ± 51 yr BP). This indicates that ^{14}C ages are not only controlled by the kind of OM protected by SA, but are also closely linked to grain size itself, which in turn argues for the importance of hydrodynamic or other physical processes associated with sedimentation (Arnarson and Keil 2007; Mollenhauer et al. 2007; Wakeham et al. 2009). ^{14}C ages of sedimentary OM increase with increasing grain size, irrespective of the acid-treatment that was applied (Figure 3). We therefore infer differences in ^{14}C ages correspond to variations in hydrodynamic properties, and specifically that grain size-dependent particle sorting effects influence ^{14}C ages. Prior studies demonstrated that the bio-diffusion coefficient varies inversely with grain size (McCave 1988; Bard 2001; Sepulcre et al. 2017). For instance, Thomson et al. (1995) concluded that the residence time in the mixed layer in deep sea sediments was particle size dependent, with coarser particles exhibit longer residence time than finer particles in low-sedimentation-rate settings (McCave 1988; Thomson et al. 1995; Brown et al. 2001). Age offsets of OM associated with different sediment grain size fractions may thus reflect hydrodynamic properties of particles both during the transport and/or its residence time in the sediment mixed layer.

Thermograms from RPO of the grain size fractions exhibit similar overall patterns that suggest a relatively homogenous carbon source, consistent with the relatively invariant δ^{13}C values of

https://doi.org/10.1017/RDC.2018.22 Published online by Cambridge University Press

the grain size fractions (~1.2‰ S.D.; Figure 2 and 4). Despite a potentially similar OC source, the thermally resolved organic components associated with each specific grain-size fraction differ in ^{14}C age to varying degrees, with the proportion and age of dominant organic components in each fraction contributing to the observed ^{14}C age of the bulk OM.

For the finer grain size fractions (i.e., <20 μm, 20–32 μm), the dominant thermal windows (e.g., $T_{1–5}$) exhibit a relatively narrow range in ^{14}C age variability (Figure 5). Notably, however, the ^{14}C ages for corresponding major thermal windows (e.g., $T_{1–5}$) systematically increase from the <20 μm to 32–63 μm fractions. Indeed this continues throughout the grain size spectrum, echoing the step-wise increase in bulk ^{14}C results (Figure 3). These results imply that the majority of OM within specific grain-size fraction experiences similar residence times in the sedimentation environment following its initial (rapid) association with specific mineral particles. This uniform ^{14}C increase with grain size may reflect hydrodynamic processes occurring in oceanic nepheloid layers. Both intermediate-depth nepheloid layers (INLs) and bottom (or benthic) nepheloid layers (BNLs) have been observed in this region (Morrison et al. 1998, 1999; Pfannkuche and Lochte 2000). Hydrodynamic influences on grain size distributions of ocean sediments are well documented (e.g., McCave 1988; Thomsen and Gust 2000; Thomsen and McCave 2000), and are likely to affect ^{14}C age characteristics of associated OM, especially in nepheloid layers where such processes are active (Inthorn et al. 2006; Mollenhauer et al. 2007; Bao et al. 2016). We suggest that "aging" (^{14}C decay) during hydrodynamically driven transport could result in systematic ^{14}C depletion of all organic components within a specific grain-size fraction, with transport times/speeds varying as a function of grain size.

In contrast to the finer fractions (<63 μm), the ^{14}C ages of different thermal windows of the coarser grain size fractions (e.g., 125–250 μm and 250–500 μm), are less uniform within a specific grain size fraction (Table 2 and Figure 5). In particular, ^{14}C ages of the most abundant thermal windows (e.g., $T_{1–5}$) increase with increasing temperature, and this trend is superimposed on the general increase in corresponding thermal windows with increasing grain size (Figure 5). Bioturbation processes are unlikely to induce significant discrepancies between ^{14}C ages of different thermal windows in specific coarser fraction given high regional surface ocean productivity, a pronounced oxygen deficient zone within the overlying water column (Pfannkuche and Lochte 2000) as well as low oxygen penetration depths (Grandel et al. 2000; Smith et al. 2000), and high accumulation rates of underlying sediments (Schnetger et al. 2000). We therefore consider two alternative explanations for this observed ^{14}C variability among thermal windows, as follows:

1. The first explanation would invoke protracted (lateral) transport and associated aging of matrix-associated OM prior to deposition, with subsequent addition of fresh (young) OM following deposition. The apparent ^{14}C aging of preassociated OM would likely reflect a combination of both lateral transport time and selective decomposition of more labile (younger) organic components. This line of reasoning is consistent with observations of Arnarson and Keil (2007) where the OM in marine sediments have experienced extensive diagenesis accumulates in the high-density (coarse) fractions. Such a scenario would imply significant timescales for development of OM associations because the ^{14}C ages of low temperature thermal windows in the coarser fractions are older than the corresponding thermal windows in the relatively finer fractions (Figure 5). Moreover, the sphericity of particles in these larger grain size fractions (Supplementary Figure S1) also implies that they have been extensively reworked (Broecker et al. 2006), and subjected to long-term influence of hydrodynamic processes during laterally transport over long distances prior to deposition.

https://doi.org/10.1017/RDC.2018.22 Published online by Cambridge University Press

2. The second explanation for the observed ^{14}C variability among thermal windows in the coarser grain size fractions would imply the presence of thermally refractory rock-derived (i.e., petrogenic) OC (i.e., ^{14}C-dead) in larger detrital grains (Figure 5, black bars (556–896° C). Rosenheim and Valy (2012) found petrogenic OC in river sediment, and identified its thermal window as >~600°C. Given significant inputs of lithogenic material to this region via both fluvial and aeolian transport (Sirocko and Lange 1991; Schnetger et al. 2000; Dahl et al. 2005) this explanation is equally plausible. Without further in-depth analyses (e.g., biomarker analysis, Raman spectroscopy), it is not feasible to determine whether one or both of these scenarios are involved, although relatively high $\delta^{13}C$ values and similar overall thermogram patterns of the coarser and finer fractions might argue against significant contributions of entrained ^{14}C-dead OM in these fractions. Nevertheless, it is clear that grain size appears to be a dominant factor controlling ^{14}C heterogeneity in Arabian Sea deep-sea sediments, and that grain size-related effects associated with transport appear to be the most plausible cause of the internal ^{14}C age variability.

In an attempt to explain our observations on the ^{14}C ages of OM in specific grain-size fractions, we propose a conceptual model that invokes different modes of OM preservation (Figure 6). In this model, finer-grained sediments (<63 μm) are mostly comprised of small (μm-scale) mineral-OM aggregates containing marine OM that is both intrinsic to the detrital particles and binds them together. Hydrodynamic processes result in parallel aging of all organic components within each grain size fraction, leading to relatively homogeneous ^{14}C ages among major RPO thermal windows. Such aggregates are likely to be metastable, with their stability related to both hydrodynamic regime and bottom water conditions (e.g., O_2 concentrations) (Inthorn et al. 2006), however these aggregates themselves may protect otherwise labile components from degradation (Arnarson and Keil 2007, reference therein). In addition, OM associated with intermediate grain sizes (e.g., silt, 32–63 μm) is relatively depleted in ^{13}C and %OC relative to other fractions (Figure 2) due to greater propensity for erosion and remobilization under lower shear stress (McCave and Hall 2006) (Figure 6), implying that sediment advection influences organic geochemical characteristics such as ^{14}C age distribution (Bao et al. 2016). For the coarser-grained (>63 μm) sediments, higher bed shear stress is required for erosion, limiting rapidly and lateral transport and redistribution under prevailing hydrodynamic conditions. For these coarser fractions, the influence of hydrodynamic processes on ^{14}C ages is intertwined due to OM encapsulation within particles. A combination of transport and deposition of encapsulated OM as well as OM that forms coatings on mineral particles during and subsequent to sedimentation may give rise to the observed age variability. Depending on particle type, material that is intrinsic to the particle may reflect marine OM (biomineral clasts; Ingalls et al. 2004) or terrestrial OM (detrital mineral grains; Eglinton et al. 2002; Dickens et al. 2004), and would be expected to be relatively impervious to degradation, even during protracted transport. In contrast, OM coating surfaces of coarser grains is likely younger, and only forms ephemeral associations due to its exposure on the grain surface and susceptibility to degradation. The interplay between these two scenarios, as well as their varying importance as a function of hydrodynamic and depositional regime, thus adds a layer of complication in the interpretations of sedimentary ^{14}C ages. This is particularly so for OM associated with coarser-grained fractions which, in contrast to the more homogeneous isotopic characteristics associated with finer-grained sediments, may contain both "stable" and "labile" forms of OM, resulting in a broader range of ^{14}C ages among thermal windows. While these conceptual models are clearly oversimplistic, they provide a framework for understanding and further investigation of relationships between sediment fabrics and the sources and isotopic characteristics of OM.

https://doi.org/10.1017/RDC.2018.22 Published online by Cambridge University Press

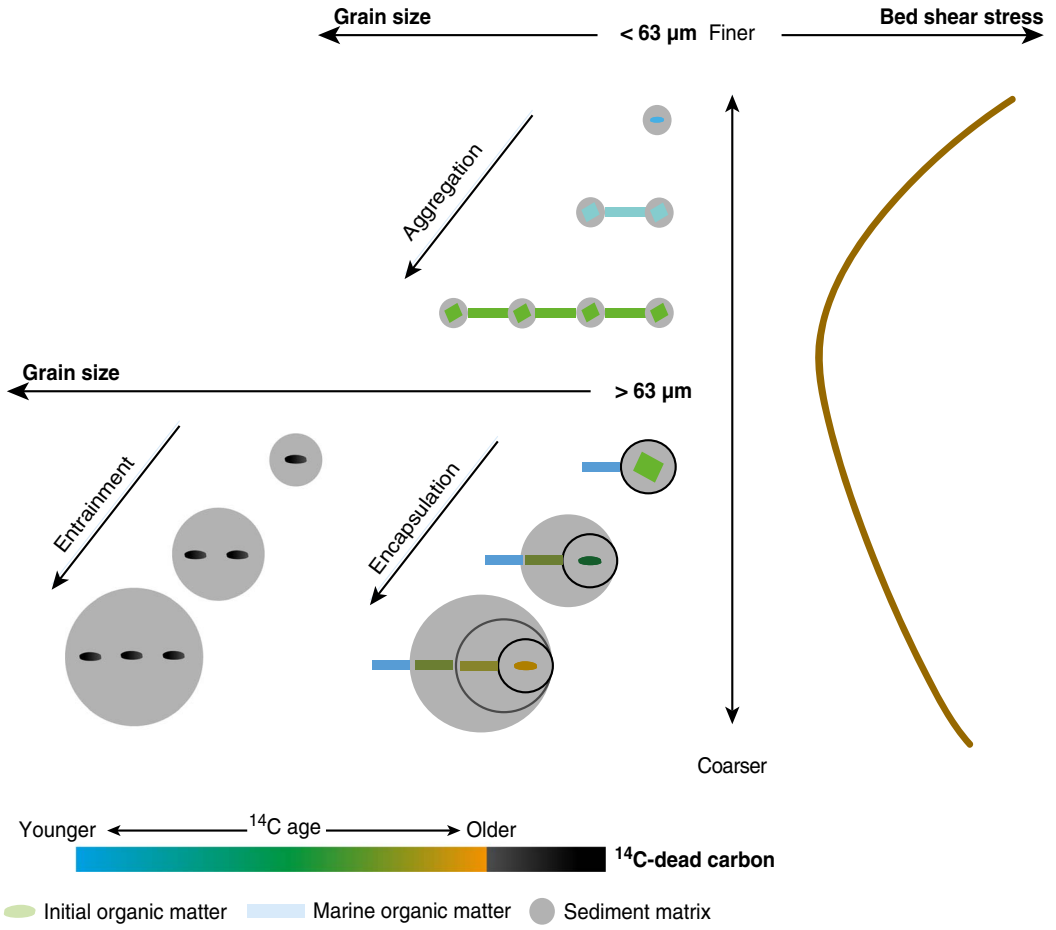

Figure 6 Conceptual model of preservation of sedimentary OM in the grain size fraction and schematic relationship between bed shear stress and grain size distribution, modified from McCave and Hall (2006).

CONCLUSIONS

- Combined ^{14}C analyses of OM in bulk sediment, specific grain size fractions, and RPO thermal OC decomposition products reveal that particle grain size is critical factor controlling in ^{14}C ages of OM in deep-sea sediment from the NW Arabian Sea.
- In this depositional setting, grain size is linked to (1) hydrodynamic processes that influence the mode and timescales of sediment and OC supply and redistribution, and (2) the spatial disposition of OM within and among sediment grains.
- Finer and coarser particle fractions exhibit contrasting degrees of ^{14}C heterogeneity. While OM derived from marine productivity is the dominant source of OC to the sediment, differing fates of OC (e.g., aggregation, encapsulation within biogenic or detrital minerals, or coating on mineral surfaces) influence its susceptibility to decomposition and resilience to physical perturbation (hydrodynamic processes), with the latter also being influenced by depositional conditions (e.g., oxygen exposure).

https://doi.org/10.1017/RDC.2018.22 Published online by Cambridge University Press

- We conclude that it is important to examine properties of different grain size and/or density fractions considering the strong influence imposed by hydrodynamic processes on the abundance, composition (including isotopic characteristics) and reactivity of sedimentary OM in the marine sediments. Further investigations, including relationships between microbial reactivity and OM ^{14}C as a function of grain size are warranted in order to better understand underlying processes.

ACKNOWLEDGMENTS

This study was supported by Doc. Mobility fellowship (No. P1EZP2_159064) (R. B.) from the Swiss National Science Foundation (SNSF). This work was also supported by SNSF "CAPS-LOCK" project 200021_140850 (T. I. E.). Additional funding came from a U.S. National Science Foundation Cooperative Agreement (OCE 0753487). We thank Julian Sachs as well as the crew of the R/V *Thomas Thompson* for enabling sample collection. We thank support of the NOSAMS staff in the execution of this project. We appreciate the assistance from members of the Laboratory for Ion Beam Physics in AMS measurements. We are grateful for the assistance of Stewart Bishop and Madalina Jaggi for stable carbon isotopic analysis at ETH Zurich.

SUPPLEMENTARY MATERIAL

To view supplementary material for this article, please visit https://doi.org/10.1017/RDC.2018.22

REFERENCES

Arnarson TS, Keil RG. 2007. Changes in OM–mineral interactions for marine sediments with varying oxygen exposure times. *Geochimica et Cosmochimica Acta* 71(14):3545–56.

Bao R, McIntyre C, Zhao M, Zhu C, Kao S-J, Eglinton TI. 2016. Widespread dispersal and aging of organic carbon in shallow marginal seas. *Geology* 44(10):791–4.

Bao Rui, Strasser M, McNichol AP, Haghipour N, McIntyre C, Wefer G, Eglinton TI. 2018. Tectonically triggered sediment and carbon export to the Hadal zone. *Nature Communications.* doi:10.1038/s41467-017-02504-1.

Bard E. 2001. Paleoceanographic implications of the difference in deep-sea sediment mixing between large and fine particles. *Paleoceanography* 16(3): 235–9.

Bergamaschi BA, Tsamakis E, Keil RG, Eglinton TI, Montluçon DB, Hedges JI. 1997. The effect of grain size and surface area on organic matter, lignin and carbohydrate concentration, and molecular compositions in Peru Margin sediments. *Geochimica et Cosmochimica Acta* 61(6):1247–60.

Blair NE, Aller RC. 2012. The fate of terrestrial organic carbon in the marine environment. *Annual Review of Marine Science* 4:401–23.

Boetius A, Ferdelman T, Lochte K. 2000a. Bacterial activity in sediments of the deep Arabian Sea in relation to vertical flux. *Deep Sea Research Part II: Topical Studies in Oceanography* 47(14): 2835–75.

Boetius A, Springer B, Petry C. 2000b. Microbial activity and particulate matter in the benthic nepheloid layer (BNL) of the deep Arabian Sea. *Deep Sea Research Part II: Topical Studies in Oceanography* 47(14):2687–706.

Brodie CR, Leng MJ, Casford JS, Kendrick CP, Lloyd JM, Yongqiang Z, Bird MI. 2011. Evidence for bias in C and N concentrations and $\delta^{13}C$ composition of terrestrial and aquatic organic materials due to preanalysis acid preparation methods. *Chemical Geology* 282(3):67–83.

Broecker W, Barker S, Clark E, Hajdas I, Bonani G. 2006. Anomalous radiocarbon ages for foraminifera shells. *Paleoceanography* 21(2): PA2008. doi:10.1029/2005PA001212.

Brown L, Cook GT, MacKenzie AB, Thomson J. 2001. Radiocarbon age profiles and size dependency of mixing in northeast Atlantic sediments. *Radiocarbon* 43(2B):929–37.

Cathalot C, Rabouille C, Tisnérat-Laborde N, Toussaint F, Kerhervé P, Buscail R, Loftis K, Sun M-Y, Tronczynski J, Azoury S. 2013. The fate of river organic carbon in coastal areas: a study in the Rhône River delta using multiple isotopic ($\delta^{13}C$, $\Delta^{14}C$) and organic tracers. *Geochimica et Cosmochimica Acta* 118:33–55.

Dahl KA, Oppo DW, Eglinton TI, Hughen KA, Curry WB, Sirocko F. 2005. Terrigenous plant wax inputs to the Arabian Sea: implications for the reconstruction of winds associated with the Indian Monsoon. *Geochimica et Cosmochimica Acta* 69(10):2547–58.

Dickens AF, Gélinas Y, Masiello CA, Wakeham S, Hedges JI. 2004. Reburial of fossil organic carbon in marine sediments. *Nature* 427(6972): 336–9.

Eglinton TI, Benitez-Nelson BC, Pearson A, McNichol AP, Bauer JE, Druffel ER. 1997. Variability in radiocarbon ages of individual organic compounds from marine sediments. *Science* 277(5327):796–99.

Eglinton TI, Eglinton G, Dupont L, Sholkovitz E, Montluçon D, Reddy C. 2002. Composition, age, and provenance of organic matter in NW African dust over the Atlantic Ocean. *Geochemistry, Geophysics, Geosystems* 3(8):1–27.

Grandel S, Rickert D, Schlüter M, Wallmann K. 2000. Pore-water distribution and quantification of diffusive benthic fluxes of silicic acid, nitrate and phosphate in surface sediments of the deep Arabian Sea. *Deep Sea Research Part II: Topical Studies in Oceanography* 47(14):2707–34.

Griffith DR, Martin WR, Eglinton TI. 2010. The radiocarbon age of organic carbon in marine surface sediments. *Geochimica et Cosmochimica Acta* 74(23):6788–6800.

Haake B, Ittekkot V, Rixen T, Ramaswamy V, Nair R, Curry W. 1993. Seasonality and interannual variability of particle fluxes to the deep Arabian Sea. *Deep Sea Research Part I: Oceanographic Research Papers* 40(7):1323–44.

Hedges JI, Keil RG. 1995. Sedimentary organic matter preservation: an assessment and speculative synthesis. *Marine Chemistry* 49(2–3):81–115.

Hemingway JD, Galy VV, Gagnon AR, Grant KE, Rosengard SZ, Soulet G, Zigah PK, McNichol AP. 2017. Assessing the blank carbon contribution, isotope mass balance, and kinetic isotope fractionation of the Ramped Pyrolysis/Oxidation instrument at NOSAMS. *Radiocarbon* 59(1): 179–93.

Hwang J, Druffel ERM. 2003. Lipid-like material as the source of the uncharacterized organic carbon in the ocean? *Science* 299:882–4.

Hwang J, Druffel ER, Eglinton TI. 2010. Widespread influence of resuspended sediments on oceanic particulate organic carbon: insights from radiocarbon and aluminum contents in sinking particles. *Global Biogeochemical Cycles* 24(4). doi:10.1029/2010GB003802.

Ingalls AE, Anderson RF, Pearson A. 2004. Radiocarbon dating of diatom-bound organic compounds. *Marine Chemistry* 92(1):91–105.

Ingalls AE, Lee C, Wakeham SG, Hedges JI. 2003. The role of biominerals in the sinking flux and preservation of amino acids in the Southern Ocean along 170 W. *Deep Sea Research Part II: Topical Studies in Oceanography* 50(3):713–38.

Inthorn M, Mohrholz V, Zabel M. 2006. Nepheloid layer distribution in the Benguela upwelling area offshore Namibia. *Deep Sea Research Part I: Oceanographic Research Papers* 53(8):1423–38.

Keil RG, Montluçon DB, Prahl F, Hedges JI. 1994. Sorptive preservation of labile organic matter in marine sediments. *Nature* 370(6490):549–52.

Keil RG, Mayer LM, Quay PD, Richey JE, Hedges JI. 1997. Loss of OM from riverine particles in deltas. *Geochimica et Cosmochimica Acta* 61(7):1507–11.

Komada T, Anderson MR, Dorfmeier CL. 2008. Carbonate removal from coastal sediments for the determination of organic carbon and its isotopic signatures, $\delta^{13}C$ and $\Delta^{14}C$: comparison of fumigation and direct acidification by hydrochloric acid. *Limnology and Oceanography: Methods* 6(6):254–62.

Kraal P, Slomp CP, Reed DC, Reichart GJ, Poulton SW. 2012. Sedimentary phosphorus and iron cycling in and below the oxygen minimum zone of the northern Arabian Sea. *Biogeosciences* 9(7): 2603–24.

Mayer LM. 1994. Surface area control of organic carbon accumulation in continental shelf sediments. *Geochimica et Cosmochimica Acta* 58(4):1271–84.

Megens L, van der Plicht J, De Leeuw J, Smedes F. 2002. Stable carbon and radiocarbon isotope compositions of particle size fractions to determine origins of sedimentary organic matter in an estuary. *Organic Geochemistry* 33(8):945–52.

McCave I. 1988. Biological pumping upwards of the coarse fraction of deep-sea sediments. *Journal of Sedimentary Research* 58(1):148–58.

McCave I, Hall IR. 2006. Size sorting in marine muds: processes, pitfalls, and prospects for paleoflow-speed proxies. *Geochemistry, Geophysics, Geosystems* 7(10):1–37.

McNichol A, Osborne E, Gagnon A, Fry B, Jones G. 1994. TIC, TOC, DIC, DOC, PIC, POC—unique aspects in the preparation of oceanographic samples for ^{14}C-AMS. *Nuclear Instruments and Methods in Physics Research B* 92:162–5.

Mollenhauer G, Inthorn M, Vogt T, Zabel M, Sinninghe Damsté JS, Eglinton TI. 2007. Aging of marine OM during cross-shelf lateral transport in the Benguela upwelling system revealed by compound-specific radiocarbon dating. *Geochemistry, Geophysics, Geosystems* 8(9) doi:10.1029/2007GC001603.

Morrison JM, Codispoti L, Gaurin S, Jones B, Manghnani V, Zheng Z. 1998. Seasonal variation of hydrographic and nutrient fields during the US JGOFS Arabian Sea Process Study. *Deep Sea Research Part II: Topical Studies in Oceanography* 45(10–11):2053–101.

Morrison JM, Codispoti LA, Smith SL, Wishner K, Flagg C, Gardner WD, Gaurin S, Naqvi S, Manghnani V, Prosperie L. 1999. The oxygen minimum zone in the Arabian Sea during 1995. *Deep Sea Research Part II: Topical Studies in Oceanography* 46(8):1903–31.

Pfannkuche O, Lochte K. 2000. The biogeochemistry of the deep Arabian Sea: overview. *Deep Sea Research Part II: Topical Studies in Oceanography* 47(14):2615–28.

Rosenheim BE, Day MB, Domack E, Schrum H, Benthien A, Hayes JM. 2008. Antarctic sediment chronology by programmed—temperature

https://doi.org/10.1017/RDC.2018.22 Published online by Cambridge University Press

pyrolysis: methodology and data treatment. *Geochemistry, Geophysics, Geosystems* 9(4) doi: 10.1029/2007GC001816.

Rosenheim BE, Galy V. 2012. Direct measurement of riverine particulate organic carbon age structure. *Geophysical Research Letters* 39:L19703. doi: 10.1029/2012GL052883.

Ruff M, Wacker L, Gäggeler H, Suter M, Synal H-A, Szidat S. 2007. A gas ion source for radiocarbon measurements at 200 kV. *Radiocarbon* 49(2): 307–14.

Schnetger B, Brumsack H-J, Schale H, Hinrichs J, Dittert L. 2000. Geochemical characteristics of deep-sea sediments from the Arabian Sea: a high-resolution study. *Deep Sea Research Part II: Topical Studies in Oceanography* 47(14):2735–68.

Schreiner KM, Bianchi TS, Rosenheim BE. 2014. Evidence for permafrost thaw and transport from an Alaskan North Slope watershed. *Geophysical Research Letters* 41:3117–26.

Sepulcre S, Durand N, Bard E. 2017. Large ^{14}C age offsets between the fine fraction and coexisting planktonic foraminifera in shallow Caribbean sediments. *Quaternary Geochronology* 38:61–74.

Sirocko F, Lange H. 1991. Clay-mineral accumulation rates in the Arabian Sea during the late Quaternary. *Marine Geology* 97(1–2):105–19.

Smith CR, Levin LA, Hoover DJ, McMurtry G, Gage JD. 2000. Variations in bioturbation across the oxygen minimum zone in the northwest Arabian Sea. *Deep Sea Research Part II: Topical Studies in Oceanography* 47(1):227–57.

Stuiver M, Polach HA. 1977. Discussion: reporting of ^{14}C data. *Radiocarbon* 19(3):355–63.

Tao S, Eglinton TI, Montluçon DB, McIntyre C, Zhao M. 2016. Diverse origins and predepositional histories of OM in contemporary Chinese marginal sea sediments. *Geochimica et Cosmochimica Acta* 191:70–88.

Thomsen L, Gust G. 2000. Sediment erosion thresholds and characteristics of resuspended aggregates on the western European continental margin. *Deep Sea Research Part I: Oceanographic Research Papers* 47(10):1881–97.

Thomsen L, McCave I. 2000. Aggregation processes in the benthic boundary layer at the Celtic Sea continental margin. *Deep Sea Research Part I: Oceanographic Research Papers* 47(8): 1389–404.

Thomson J, Cook G, Anderson R, Mackenzie A, Harkness D, McCave I. 1995. Radiocarbon age offsets in different-sized carbonate components of deep-sea sediments. *Radiocarbon* 37(2):91–101.

Trumbore SE, Zheng S. 1996. Comparison of fractionation methods for soil organic matter ^{14}C analysis. *Radiocarbon* 38(2):219–29.

Turnewitsch R, Witte U, Graf G. 2000. Bioturbation in the abyssal Arabian Sea: influence of fauna and food supply. *Deep Sea Research Part II: Topical Studies in Oceanography* 47(14):2877–911.

Wakeham S, Canuel E. 2016. The nature of organic carbon in density-fractionated sediments in the Sacramento-San Joaquin River Delta (California). *Biogeosciences* 13(2):567–82.

Wakeham SG, Canuel EA, Lerberg EJ, Mason P, Sampere TP, Bianchi TS. 2009. Partitioning of organic matter in continental margin sediments among density fractions. *Marine Chemistry* 115(3):211–25.

Wang X-C, Druffel ERM. 2001. Radiocarbon and stable carbon isotope compositions of organic compound classes in sediments from the NE Pacific and Southern Oceans. *Marine Chemistry* 73:65–81.

Wang X-C, Druffel ERM, Griffin S, Lee C, Kashgarian M. 1998. Radiocarbon studies of organic compound classes in plankton and sediment of the northeastern Pacific Ocean. *Geochimica et Cosmochimica Acta* 62:1365–78.

Wang X-C, Druffel ERM, Lee C. 1996. Radiocarbon in organic compound classes in particulate OM and sediment in the deep northeast Pacific Ocean. *Geophysical Research Letters* 23:3583–6.

Zigah PK, Minor EC, McNichol AP, Xu L, Werne JP. 2017. Constraining the sources and cycling of dissolved organic carbon in a large oligotrophic lake using radiocarbon analyses. *Geochimica et Cosmochimica Acta* 208:102–18.